THE EFFECTS OF ANEUPLOIDY ON POSTERIOR DEVELOPMENT IN *DANIO RERIO*

A Thesis
by
ABIGAIL SHAW HOCKETT

Submitted to the Graduate School
at Appalachian State University
in partial fulfillment of the requirements for the degree of
MASTER OF SCIENCE

May 2023
Department of Biology

THE EFFECTS OF ANEUPLOIDY ON POSTERIOR DEVELOPMENT IN *DANIO RERIO*

A Thesis
by
ABIGAIL SHAW HOCKETT
May 2023

APPROVED BY:

Mary D. Kinkel, Ph.D.
Chairperson, Thesis Committee

Cortney M. Bouldin, Ph.D.
Member, Thesis Committee

Andrew C. Bellemer, Ph.D.
Member, Thesis Committee

Ava J. Udvadia, Ph.D.
Chairperson, Department of Biology

Marie Hoepfl, Ed.D.
Interim Dean, Cratis D. Williams School of Graduate Studies

Abstract

THE EFFECTS OF ANEUPLOIDY ON POSTERIOR DEVELOPMENT IN *DANIO RERIO*

Abigail Shaw Hockett
B.A., Furman University
M.S., Appalachian State University

Chairperson: Mary D. Kinkel, Ph.D.

This research focuses on understanding how aneuploidy affects development. Aneuploidy is the state of having more or fewer sets of chromosomes than what naturally occurs in the organism. In cases of aneuploidy, the altered number of chromosomes is associated with proportional changes in cell volume. To address this question, the zebrafish is an ideal model. Their external fertilization allows us to observe development from the one-cell stage. Protocols were developed for generating haploid and tetraploid embryos. This allowed a comparison of embryonic development between normal diploid embryos versus haploid and tetraploid embryos with half or double the normal number of chromosomes, respectively. The altered chromosome number was confirmed using karyotyping. Analysis of the gross morphology of the embryos at 24 hours post fertilization found haploid and tetraploid embryos to have shortened and malformed posterior bodies. Next, *in situ* hybridization was performed to determine whether gene expression was affected in the somites (blocks of developing muscle) or somite boundaries. Expression of *myod1* was disrupted in haploid and tetraploid embryos, indicating defects in normal muscle development. Similarly, expression of *xirp2a* showed disruptions to the somite boundaries. These results support the hypothesis that aneuploidy affects posterior development by causing defects in somite development. These findings are supported by the growing interest in mechanical forces in development.

Acknowledgments

I would like to thank Cortney Bouldin, for the opportunity to work in his lab and the project that he laid out for me. I would also like to thank Mary Kinkel for her willingness to accept me into her lab and for all the guidance she provided. Additionally, I would like to thank my other committee member, Andrew Bellemer, for his insight and encouragement. I would like to express gratitude to the other members of the Bouldin/Kinkel lab, Joey Manuel, Elsie Rodriguez, and Wayne Blanchett, for initiating me into the lab experience, their research that I enjoyed building off of, and for their assistance in maintaining the health of our fish. I would also like to thank Guichuan Hou for all of his assistance in the microscopy facility, and general willingness to accept my presence there. I also have gratitude for all my fellow students in the graduate program, for lending their support and commiseration for all our efforts and aspirations. I extend my thanks to the Office of Student research, for their support in funding my research. I also extend gratitude to Biorender for the use of their tool to create graphics and figures.

Table of Contents

List of Figures

INTRODUCTION

Vertebrates are chordates with a backbone, including animals such as humans, birds, mammals, reptiles, and fish. *Danio rerio*, or zebrafish, is an ideal model organism for studies in the development of vertebrates. Due to the mode of fertilization and the transparency of the embryo, development can be carefully monitored. Eggs are fertilized externally, meaning that eggs are fertilized by the male's sperm after the egg has been released from the female's body. This allows development to be observed from the single-cell stage throughout the course of development (Figure 1). All this is able to be viewed in real-time through a simple light microscope, allowing for an in-depth analysis of the development process from the very beginning.

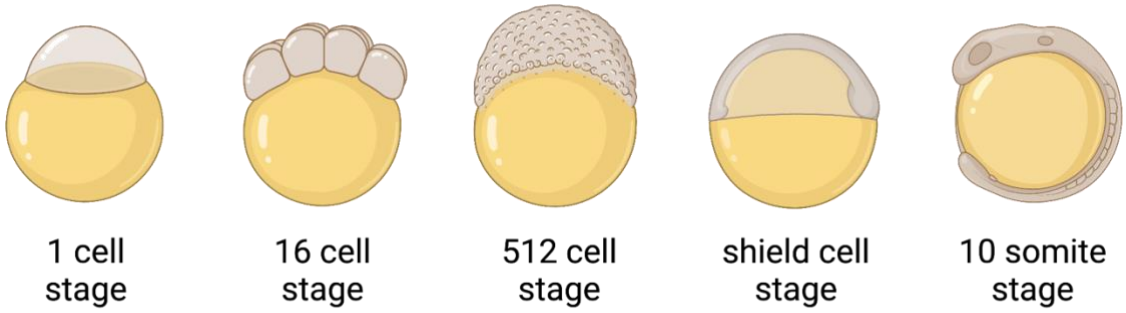

Figure 1. Zebrafish embryo development from the 1 cell stage to the 10 somite stage.

Posterior development

An important element in the development of vertebrates is establishing and extending the anteroposterior axis (Dubrulle and Pourquié, 2004). Along this axis, the vertebrae are formed, the defining characteristic of vertebrate organisms. Posterior development in zebrafish is often identified as the body's development beyond the head (Kimelman, 2016). In the zebrafish, posterior development begins to be obvious at the tailbud stage, at 10 hours

post fertilization (hpf). During this stage, the head and tailbud are becoming more identifiable. Based on the figure below, the head is oriented at the top and the tail below. Beyond this stage, the axis becomes more defined and the posterior body extends past the yolk ball and yolk extension (Figure 2).

Figure 2. Zebrafish embryonic development from the bud stage to the prim-6 stage.

Somitogenesis

The development of the posterior body begins with the generation of somites. These are bilateral tissue blocks that develop first in the trunk of the embryo and later extend along the tail, one pair at a time. Every 30 minutes, another pair of somites is added posteriorly. As somitogenesis progresses, the somites at the very end of the tail form more slowly. At the prim-5 stage the last pair of somites forms at the tip of the tail, ending with about 30-34 somite pairs in total (Kimmel et al., 1995; Schröter et al., 2008). The process of the development of these segments is known as somitogenesis. The somites begin as blocks of undifferentiated tissue that later develop into skeletal muscle, vertebral bone, ribs, cartilage, and dermis (Wolpert et al., 2007). Beginning in the anterior just behind the head, somites are formed in the posterior direction extending the anteroposterior axis (Figure 3A). Somites are developed in pairs that bracket the neural tube, the precursor to the central nervous system,

and the notochord, a cartilaginous structure important for signaling tissue differentiation and structural support for the growing embryo. Somites are also bordered laterally by undifferentiated tissue known as the lateral plate mesoderm (Figure 3B) (Stickney et al., 2000).

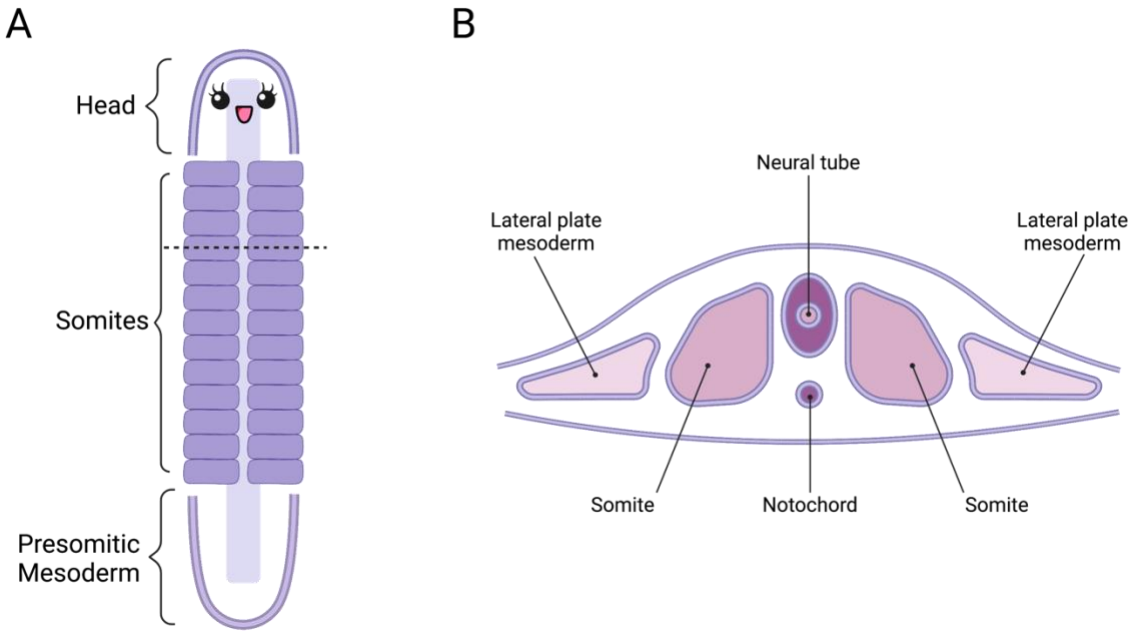

Figure 3. Segmentation of the body axis through somitogenesis. (A) Diagram showing the body plan during somitogenesis. Dashed line indicates the position of the cross-sectional image in (B) Cross-section through a 24 hpf embryo.

The first somite is formed just after the end of gastrulation, around 10.5 hpf, marking the shift into somitogenesis. Somites form from the anterior presomitic mesoderm (PSM) while the PSM continually adds on more cells and extends in the posterior direction. The PSM refers to the unsegmented region of precursor tissues that undergo somitogenesis (Wolpert et al., 2007). The positional identity of somitic cells is determined during gastrulation. The unsegmented PSM has already specified the identity and positioning of the blocks that will form into somites. The rhythmic generation of somites from the PSM is

regulated by a mechanism of cyclic gene expression known as the segmentation clock (Oates et al., 2012). While a full understanding of all the contributors to the segmentation clock is unknown, many key players have been identified.

Segmentation clock

This pre-patterning for somites is accomplished through the cyclical expression of genes in various signaling pathways (Wolpert et al., 2007). The oscillating nature of gene expression is most commonly depicted through the use of the Clock and Wavefront model (Cooke and Zeeman, 1976). The clock aspect of the model describes oscillations in gene expression throughout the PSM, creating a pattern of gene expression down the PSM. The wavefront mechanism describes how a record of these oscillators is kept as the "wavefront" moves through the PSM from anterior to posterior. The wave acts as a determinant, deciding the identity of the cells as it passes through the PSM, in the wake of the wavefront is the patterning that aligns with the somites-to-be (Figure 4) (Cooke and Zeeman, 1976; Dubrulle and Pourquié, 2004). The periodicity of the waves of expression in the segmentation clock is equivalent to the formation of each pair of somites (Stickney et al., 2000). Thus, the segmentation clock is critical for the proper patterning of segments along the anteroposterior axis. Even the timing of the segmentation clock is crucial. A study by Schröter and Oates (2010) determined that slowing the segmentation clock could result in an increase in somite length and a decrease in somite number.

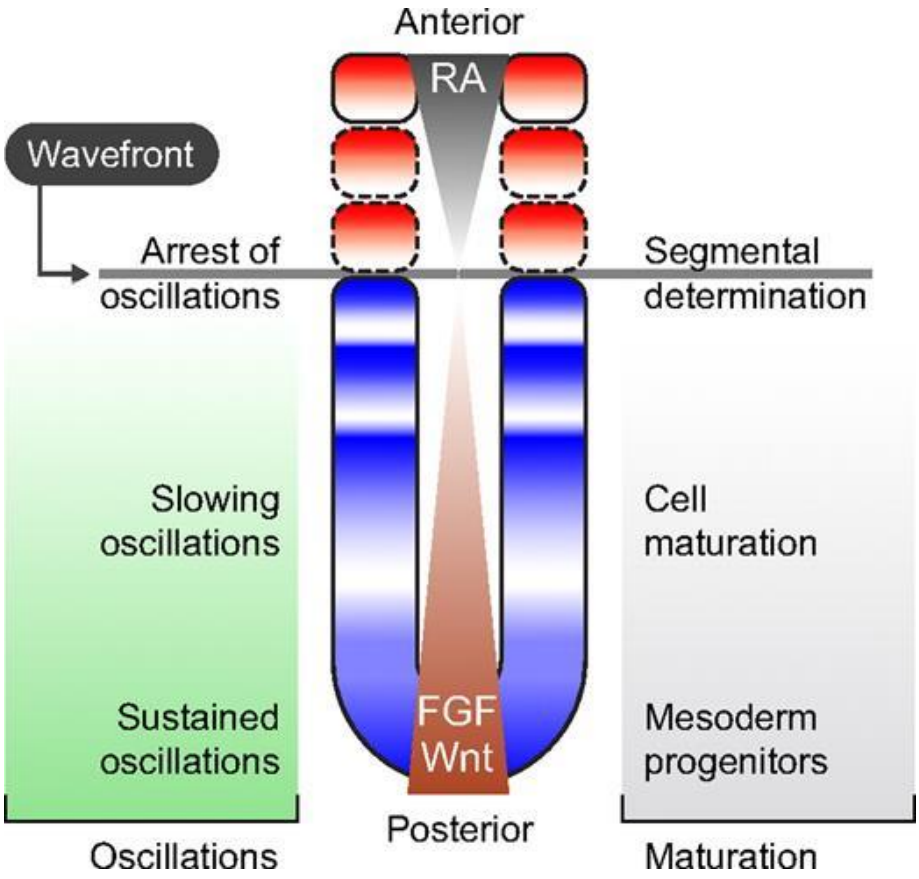

Figure 4. Schematic of clock and wavefront model. Model displays the tailbud region of the embryo, with cyclic gene expression in blue/white, arrested segments and somites in red/white. This schematic comes from Oates et al., 2012.

When this model was first put forward, there were no clear identities of the oscillators that pattern the position of embryos. It is only in the past couple of decades that they have been identified. Some important players amongst many vertebrate organisms include the Notch-Delta pathway, the *Hes/Her* family, fibroblast growth factor, and *mesp* genes (Sawada et al., 2000; Oates et al., 2012; Yabe and Takada, 2016). The expression of Notch-Delta genes paired along with *Hes/Her* gene family generates a negative feedback loop that helps define the anterior and posterior regions of the future segments. Notch-Delta signaling is necessary for the synchronicity of oscillations between neighboring cells, promoting synchronicity of the segmentation clock (Holley, 2007; Yabe and Takada, 2015). However,

there are many questions that are left unanswered by the clock and wavefront model. For instance, how the clock and wavefront model acts on a cellular level is still not fully understood. There are many questions surrounding the extent of cell movement that occurs in the tailbud during the period of posterior expansion in the PSM that cannot be answered with the present model. How these intricate dynamics still allow for tissue synchronicity is of great interest (Bhavna, 2020). More recent work has suggested a multicellular clock that acts based on local interactions to then lend aid in morphogenesis (Uriu et al., 2021).

Somite boundaries

Somite boundary formation begins when somites form from the PSM. Boundaries are established that clearly define the anterior and posterior borders of the somites. The process of boundary formation begins early in the development of the somite as part of the mesenchymal to epithelial transition (MET). During this transition, the blocks of somitic tissue become epithelialized along the lateral edges, leaving a mesenchymal center to the somite, much of which will differentiate into the myotome. The epithelialization of the outer cells of the somite assists in creating a physical separation between adjacent somites (Henry et al., 2005). Following the MET, the somite boundaries develop a rich extracellular matrix. Some of the prominent constituents in the somite boundary are a fibronectin network, a laminin and actin matrix, cadherin proteins, and β-catenin (Holley, 2007).

Early somites are cuboidal in shape. As the somite boundaries develop connections and create tension, the somites lengthen and assume the chevron shape (Figure 5). The development of the chevron shape is primarily thought to be due to the tension and resistance created between somites at their borders (Rost et al., 2014; Naganathan and Oates, 2020).

These boundaries set limits to myofibers that are elongating to extend the length of the somites, assisting in the proper development of the myotome (Henry et al., 2005). All this contributes to how somite boundaries are crucial for the proper formation of the posterior body.

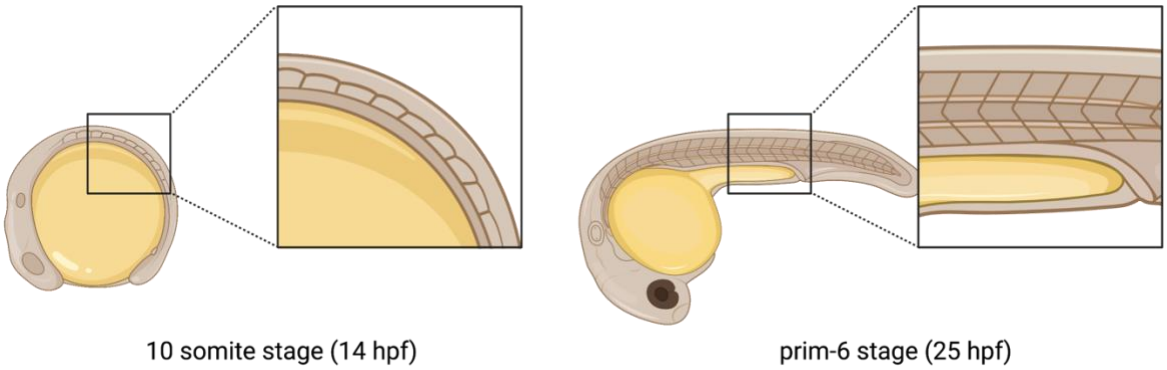

Figure 5. Cuboidal to chevron shape development in somites. A closer look at normal somite morphology over time.

Cell migration and mechanical influences

While the segmentation clock model has been the hallmark of understanding somitogenesis and the development of the posterior body, more recent studies have focused on understanding the role of cell movements and mechanics in posterior body formation. Many of these studies consider the influence of cell size in the proper migration and positioning of cells during development.

A study by Menon et al., (2020) concluded that cell size is crucial to proper embryo formation. Finding that the influence of cell size in gastrulation had not yet been studied in any model organism, they worked to determine the relative importance of cell size. By inducing a change in cell size via ploidy manipulation, the study determined that embryos with cell sizes that deviate from the norm show gastrulation defects. The conclusion was that

these defects were due to the cells' inability to migrate to their proper position during gastrulation. Noting the limited change in gene expression during early development (3-8 hpf), the study posits that the deficiencies in development ultimately result from improper collective cell migration due to changes in cell size. To gauge the effects of altered cell size later in development, after gastrulation and when the body axis has been formed, embryos were raised to 30 hpf and their gross morphologies were observed. The aberrant morphologies primarily consisted of shortened body axes both in embryos with smaller cells and embryos with larger cells than what is normal (Menon et al., 2020). This research was centered around understanding how cell size and collective cell migration influence gastrulation. While they did not look at the result of these influences in later-stage embryos, these findings could also explain the defects seen in later development.

Recent studies have also begun to investigate the importance of multi-tissue mechanics and their potential effects on developing embryos. As somitogenesis is occurring, the notochord is following a path of growth with the addition of new notochord cells at the posterior end while cells at the anterior mature. The development of the notochord includes vacuolation of cells in the anterior. This vacuolation begins in the anterior and progresses toward the posterior end of the notochord. The work done by McLaren and Steventon (2021), showed that the development of the notochord is necessary for the proper elongation of the posterior axis in zebrafish embryos. Without the presence of the notochord and its elongation, somites will not extend properly. Mechanical influences on posterior development have even been shown to affect the left-right symmetry of the posterior axis (Rost et al., 2014; Naganathan et al., 2022). In early somitogenesis, the patterning between the pairs of somites is not exactly symmetrical after their initial formation, though it is

recovered within an hour in wildtype embryos. The initial asymmetry is due to the segmentation clock only providing general spatiotemporal designations for the tissue of each somite. This asymmetry is then resolved by surface tension and other external stresses from nearby tissues (Naganathan et al., 2022).

Studying the formation of somites in zebrafish has provided a unique opportunity to observe tissue separation and the formation of boundaries *in vivo*. The relevance of mechanics in the proper formation of somites is becoming more apparent, though there are still many details left unknown, such as the prominent processes of boundary formation occurring sequentially or concurrently (Naganathan and Oates, 2020). With the zebrafish proving to be an ideal model for the study of cell and tissue mechanics during development, there are many reports being published beginning to address these new areas of interest.

Effects of cell size on development

Along with the new line of inquiry involving the influence of mechanics on posterior development, the effects of cell size have also become of interest to many researchers. As discussed previously, Menon et al. (2020) based their study on the influence of cell size during gastrulation. Menon et al. generated embryos with abnormal cell sizes by manipulating ploidy, the number of sets of chromosomes (2020). Humans, and zebrafish alike, are diploid organisms that have two of each chromosome. When a cell or organism has chromosome numbers that differ from the norm it is known as aneuploidy. A primary characteristic of aneuploid organisms is a change in cell size. Cells with double the normal DNA are larger in volume, and cells with half the normal DNA content have smaller volumes (Menon et al., 2020; Rodriguez, 2020; van de Pol et al., 2021) It is also relevant to note that

although the cell volumes may be larger or smaller, this does not mean that the full length of the embryo is smaller or larger to the same degree. Though they are shorter, haploid embryos are not half the size of a diploid embryo. The embryo is shown to have more cells than a wildtype embryo, allowing the embryo to maintain a more "normal" size. Tetraploid embryos also maintain a more normal size by having fewer cells. Like haploid embryos, tetraploid embryos have a shorter body axis than wildtype diploid embryos (Walker, 1999; Rodriguez, 2020)

The primary attributes associated with haploid embryos are a shortened body axis, heart edema, and a failure to inflate the swim bladder. Amongst other defects, haploid embryos have been shown to not live longer than 5 days (Walker, 1999). In terms of posterior development, it has been stated that haploid embryos have the same number of somites as diploid embryos. Aside from the observations noted here, there is little literature focused on understanding the specifics of haploid embryo malformation and how it occurs (Walker, 1999; Kroeger et al., 2014).

A recent master's thesis on aneuploidy and its influence on neuromesodermal progenitor cells provided data concerning the defects in morphology in both tetraploids and haploid embryos in the time periods following gastrulation (Rodriguez, 2020). To gauge the lasting effects of aneuploidy, embryos were analyzed at five days post-fertilization. At this time point the body axis has been fully extended and the embryos have entered into the larval phase of growth. Body length measurements of haploid and tetraploid embryos were taken and compared to wildtype diploid larvae. Haploid embryos were 1.8 times shorter in comparison to the diploid controls. Tetraploid embryos were 1.125 times short in comparison to the diploid controls. Along with a statistically significant decrease in body length, the

tetraploid larvae were also noted for having variability in their phenotypes. Tetraploids were shown to have varying degrees of abnormalities, ranging from curved body axes and underdeveloped eyes, to morphologies that closely resembled the diploid larvae (Rodriguez, 2020). With this information, it is clear that aneuploidy is associated with morphological defects in developing embryos. My research is focused on understanding the ways in which aneuploidy disrupts the development of the posterior body.

AIMS

The objective of this study is to better understand the ways in which aneuploidy affects the posterior development of zebrafish. In order to do so, I developed two principal aims for my research. The first aim was to demonstrate that aneuploidy results in defects in the posterior body of zebrafish embryos. The second aim was to show that aneuploidy disrupts somite formation. To do all this, I generated aneuploid embryos and examined their gross morphology, and then gauged the defects in somite formation through analysis of gene expression.

METHODS

Zebrafish husbandry

Zebrafish were a wild-type variety from a local pet shop. All zebrafish procedures were approved by the Appalachian State University Institutional Animal Care and Use Committee. Fish were housed in an Aquaneering system in the Bouldin/Kinkel lab in the vivarium facility. Water quality was tested weekly, with the pH being taken daily and maintained at 6.8-7.2 pH. The temperature in the system was kept between 27ºC to 28ºC. While the aim was to keep conductivity between 600-850 microsiemens, due to some filtration issues, the conductivity was maintained at 800-1000 microsiemens. Fish were fed dry food at 9:00AM and 48-hour old brine shrimp (*Artemia franciscana*) at 3PM. The zebrafish were kept on a 14-hour light cycle from 9:00AM to 11:00PM.

In vitro fertilization

To control the timing of fertilization, *in vitro* fertilization was performed as previously described (Westerfield, 2000). Males with healthy yellow coloring and females with distended abdomens were selected for *in vitro* fertilization. Six males and females were kept separately in breeding tanks the evening prior to *in vitro* fertilization. Males and females were anesthetized in roughly 50 mL of 1X Tricaine, made from a 25X Tricaine stock solution diluted with fish facility water. Once anesthetized, males were dried by dabbing with a Kim wipe, then mounted ventrally on a foam plug that had a small slit on the top. The foam plug was held on a dry 9 cm petri dish. A 10 µL capillary tube was placed between the anal fins, by the cloaca, and gentle pressure was applied down the abdomen toward the cloaca. The gentle pressure expelled the sperm which was then collected in the capillary tube. The male

was then returned to the recovery tank and the sperm was immediately transferred into an Eppendorf tube with 10 µL Hanks solution (0.137 M NaCl, 5.4 mM KCl, 0.25 mM Na_2HPO_4, 0.44 mM KH_2PO_4, 1.3 mM $CaCl_2$, 1.0 mM $MgSO_4$, and 4.2 mM $NaHCO_3$) and held on ice until needed.

Once females were anesthetized, they were dried by dabbing with a Kim wipe and laid laterally in a dry petri dish. Gentle pressure was applied along the abdomen towards the cloaca, expelling the eggs. Eggs were collected by gently using a spoon and the female was immediately returned to a recovery tank. Within 30-40 seconds of collecting the eggs, the sperm solution was deposited onto the eggs, followed by addition of 1 mL of embryo media (EM) (15.0 mM NaCl, 0.838 mM KCl, 0.0528 mM Na_2HPO_4, 0.147 mM KH_2PO_4, 1.29 mM $CaCl_2$, 0.994 mM $MgSO_4$ x $7H_2O$, and 0.714 mM $NaHCO_3$). The eggs were gently mixed in the sperm solution and EM using a capillary pipette tip. After two minutes, the eggs were fully immersed in EM and placed into a 28.5°C incubator.

Ploidy Manipulation

Haploid production with UV treatment

The generation of haploid embryos was achieved through UV irradiation treatment of the sperm, as can be seen in Figure 6A (Streisinger et al., 1981, Westerfield, 2000). Prior to females being squeezed for eggs, sperm in the Hanks solution was transferred to a depression slide under the UV lamp. The sperm was treated with the UV for two minutes and then transferred to a new Eppendorf tube and kept on ice until needed for fertilization.

Tetraploid production with heat shock

A two-minute heat shock at 41.5°C was used to generate tetraploid embryos, following the protocol described by Heier et al., 2015 and shown in Figure 6B. Embryos were fertilized by *in vitro* fertilization, as described above, and held in a 28.5°C incubator until the time for heat shock. Prior to heat shock, the embryos were transferred to a Falcon 40 µm nylon cell strainer which was held in an 100 mL culture dish with pre-warmed 28.5°C EM. At 22 minutes post-fertilization (mpf), the embryos were heatshocked by transferring the strainers to a pre-warmed culture dish with EM at 41.5°C in a water bath. Following a two-minute heat shock, the embryos were removed from the dish by lifting the strainers. Excess EM was blotted from the strainers on a paper towel and the embryos were immediately returned to the culture dish in the 28.5°C incubator. Shortly afterward, at around 30 mpf, the embryos were moved from the strainers and placed back in their normal culture dish, and allowed to develop normally.

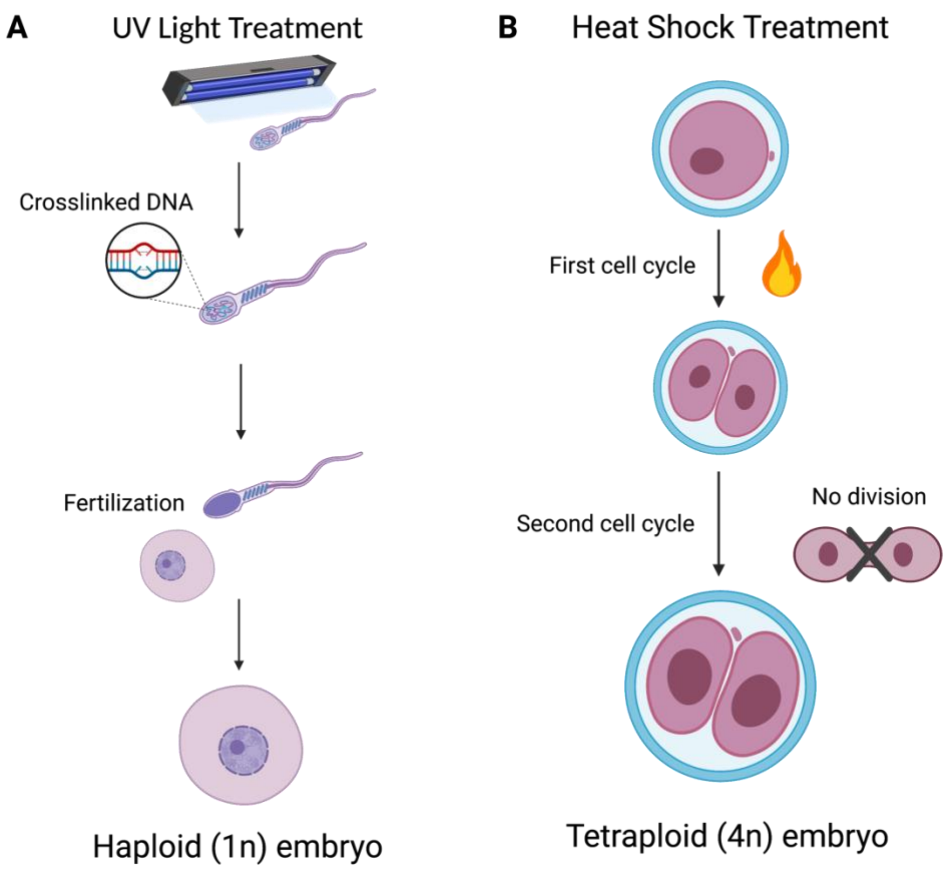

Figure 6. Ploidy manipulations. A) Haploid embryos were generated through UV irradiation of the sperm. Irradiation crosslinks the DNA, preventing the sperm from contributing genetic material to the egg. B) Tetraploid embryos were generated by heat-shocking fertilized eggs during the first cell cycle. The heat shock causes a stall in the second cell cycle resulting in cells with double the normal amount of genetic material.

At 50-65 mpf, the treated embryos were sorted based on appearance, the various states are depicted in Figure 7. Embryos with two cells indicated that the second cell cycle was successfully stalled, identifying them as tetraploid embryos. The two-celled embryos were separated for further studies. Embryos with three cells indicated an incomplete stall in cell division and these were discarded. Embryos with four cells indicated an ineffective heatshock, allowing the cells to complete their second cell division normally. These embryos were also separated and discarded.

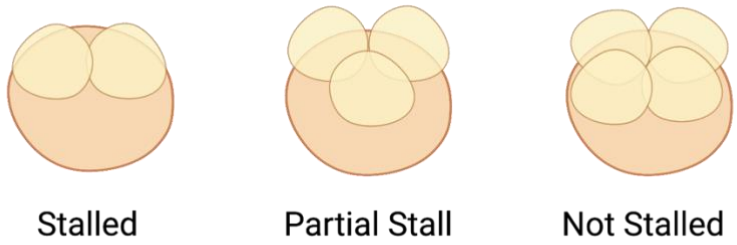

Figure 7. Phenotypes of embryos at 50-60 minutes post fertilization, following heat shock treatment. Sorting among these phenotypes allows selection of tetraploid embryos.

Karyotyping

In order to confirm the ploidy of the manipulated embryos, karyotyping was performed to visualize and count the number of chromosomes. The karyotyping protocol from Asana Marican et al., in 2021, was followed with the exception of the use of colcemid instead of colchicine to stall cells in metaphase. Embryos were prepared as described above and raised to 24 hpf at 28.5°C. At 24 hpf the embryos were transferred to Eppendorf tubes (~20 embryos/tube) and covered in 0.1 µg/mL colcemid in EM and incubated for 90 minutes at 28.5°C. Following colcemid treatment, the embryos were incubated in 1% Na Citrate in EM to encourage the cells in the embryo to swell. While in Na Citrate, the embryos were deyolked using forceps and a syringe needle. Finally, embryos were fixed in 3:1 Methanol: Glacial acetic acid (Carnoy's solution) and stored in the freezer until needed for slide preparation.

Prior to creating metaphase spreads, embryos were divided into one embryo per tube with a small amount of Carnoy's solution. Using a 20 µL pipette tip, the embryo was homogenized into a cell suspension, with a new pipette tip being used for each embryo. 25 x

75 x 1 mm microscope slides were prepped by soaking them in reverse osmosis (RO) H_2O at 4°C. Slides were dried with Kim wipes and rested on top of a flat ice pack and chilled. From ~8 inches above, the cell suspension from one embryo was dropped onto a slide, encouraging the cells to burst upon impact. Slides were held over a hot water bath to spread the chromosomes and prepped for staining. Chromosomes were stained with 1:15,000 DAPI:PBS and mounted with an EMS Glycerol Mounting Medium with DABCO™, an antifade mounting medium. Slides were then coverslipped, and the edges were sealed with clear nail polish.

In situ hybridization

Whole-mount *in situ* hybridization was performed as previously described (Thisse et al., 2004). Briefly, probes were labeled with digoxigenin (DIG) and the complementing antibodies were conjugated to alkaline phosphatase. NBT/BCIP was the substrate used to visualize the probe.

Imaging and Processing

Metaphase spread images were taken using a Zeiss Laser Scanning Microscope (LSM) 880, using a 405 nm laser diode and a 63X objective. Z-stack images were generated using ZEN 2.3, and were analyzed and processed using ImageJ.

Embryos assessed for gross morphology were in a depression slide and submerged in an 80% glycerol solution in PBST. The images were visualized on a Huvitz HSZ-ZB700 stereomicroscope with a 1X objective and 2.5 zoom for all images, and taken with a Canon EOS Rebel T6i camera.

Whole mount *in situ* hybridized embryos were mounted between bridged coverslips and submerged with 80% glycerol solution in PBST. Images were taken using an Olympus IX81 inverted microscope with an Olympus DP80 camera and 10X objective. Images were viewed and processed with Olympus cellSens Dimension 1.16.

RESULTS

The initial aim of this study was to determine whether aneuploidy disrupts posterior development. To start, it was necessary to generate embryos with altered ploidy. Chromosome number was manipulated in fertilized eggs to produce haploid and tetraploid embryos. To produce haploid embryos, sperm was collected from adult males, the DNA was damaged using UV light, and then eggs were mock fertilized with the damaged sperm. The remaining embryos were grown to the 24 hour post fertilization (hpf) stage and then analyzed for gross defects. A subset of the 24hpf embryos was used for karyotyping to confirm haploidy. Tetraploid embryos were generated using a heat shock protocol that prevented the second cell cycle division, thus doubling the number of chromosomes. Again, the embryos were grown to 24 hpf and analyzed for gross defects, while a subset of these embryos was used for karyotyping to confirm tetraploidy.

To confirm that a published karyotyping protocol would be successful, diploid embryos were processed by stalling cells during metaphase, creating a cell suspension, and spreading the chromosomes on slides for analysis. Counting the chromosomes confirmed the expected 50 chromosomes for diploid embryos (Figure 8). I then went on to karyotype the manipulated embryos. Karyotyping confirmed that UV-treatment produced haploid embryos with 25 chromosomes (Figure 9A, A'), and heat shocking produced tetraploid embryos with 100 chromosomes (Figure 9B, B').

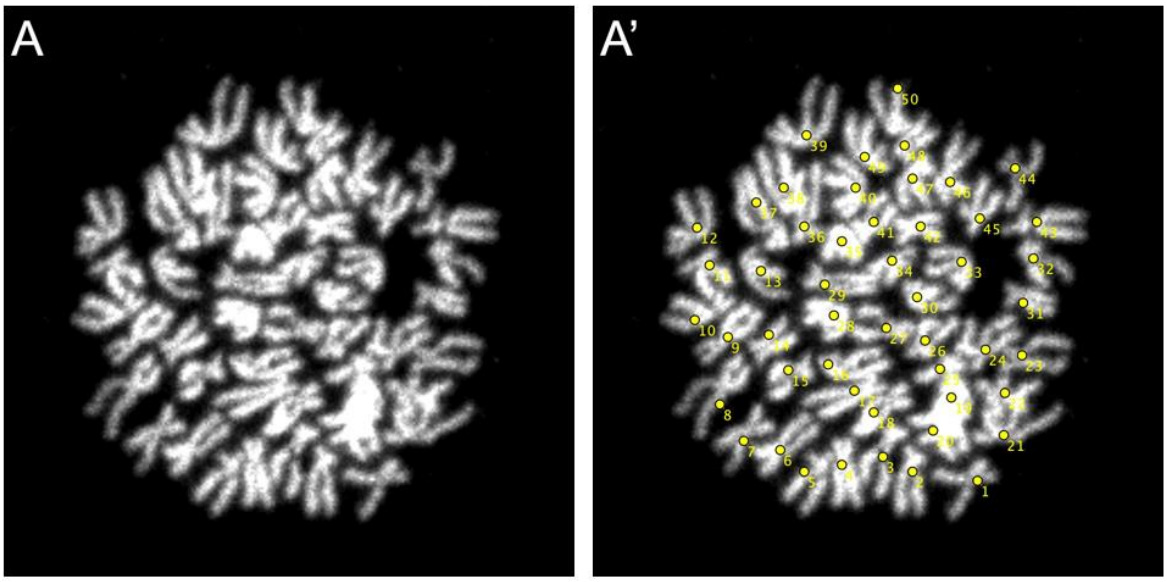

Figure 8. Metaphase chromosome spread from a diploid embryo. (A) Chromosomes from one nucleus. (A’) Counting shows 50 chromosomes, confirming diploidy, (2n).

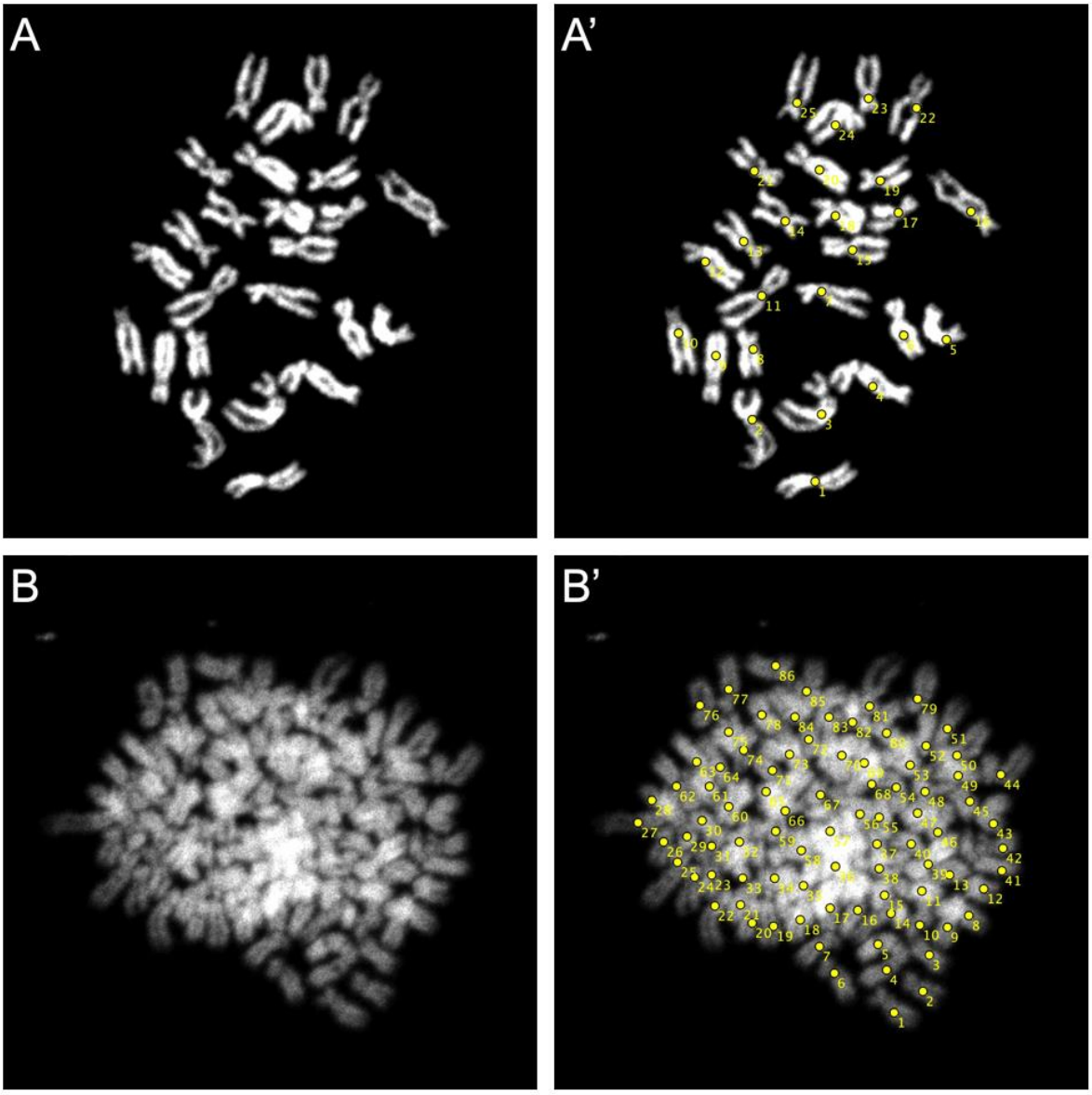

Figure 9. Metaphase chromosome spreads from manipulated embryos. (A) Chromosomes from one nucleus of a haploid embryo. (A') Counting shows 25 chromosomes, confirming haploidy (1n). (B) Chromosomes from one nucleus of a tetraploid embryo. (B') Counting shows 100 chromosomes, confirming tetraploidy (4n).

Next, the aneuploid embryos were imaged after 24 hours of development to determine whether there were obvious defects in gross morphology. Previous studies have noted that aneuploidy affects posterior development, characterized by a shorter body and trunk (Kroeger et al., 2014). In the current study, posterior defects in gross morphology were observed, consistent with previous reports. All haploid embryos showed delayed

development that included a shortened body axis compared to diploid embryos (Figure 10A, B). Haploid embryos had shortened tails, shortened yolk extensions, and often displayed posterior curvature. Unexpectedly, some tetraploid embryos showed either no obvious gross defects or modest curvature of the posterior tail (Figure 10C). Other tetraploid embryos displayed shortened tails or curved tails, or both (Figure 10D, E). Commonly, tetraploid embryos showed delayed development such that at 24 hpf they appeared to be at the 20 – 22 hpf stage, as illustrated in Figure 10F.

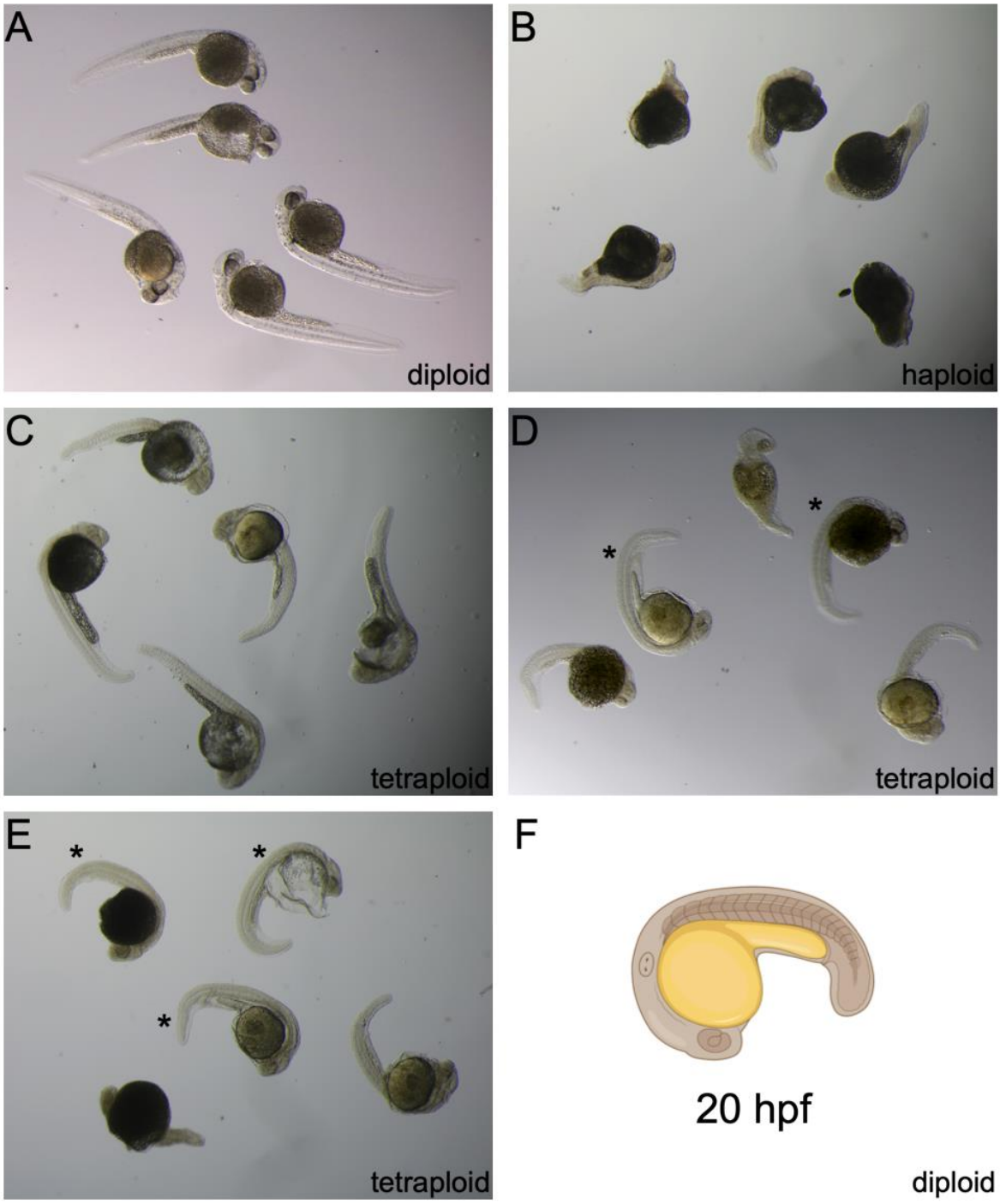

Figure 10. Gross morphology differences at 24 hpf between embryos with different ploidy levels. (A) diploid (n=15), (B) haploid (n=20), and (C-E) tetraploid embryos (n=25). (F) Schematic of a diploid embryo at 20 hpf. Asterisks indicate tetraploid embryos with delayed development. All panels are at the same magnification.

The secondary aim of this study was to confirm that aneuploidy results in aberrant somite development. Given the morphological defects that result from aneuploidy, it is clear that somite development has been disturbed in some way. To test this, whole mount in situ hybridization was performed using probes to label the somite boundaries and the developing muscle of the somitic mesoderm. Embryos were hybridized with an antisense probe for *xirp2a* (*xin actin binding repeat containing 2a*) to detect potential defects in somite boundaries. In wildtype embryos at 24 hpf, this marker revealed the expected chevron pattern between each somite pair (Figure 11A). In haploid embryos, the boundaries were labeled, suggesting that distinct blocks of somitic tissue were present. However, in posterior regions the characteristic chevron pattern was less apparent than in diploid embryos (Figure 11B-D). In the developing tail, the *xirp2a* labeling showed more linear boundaries in the dorso-ventral axis. Additionally, the boundaries appeared to be closer together, suggesting that the somites were smaller in the anterior-posterior direction. Further, in some embryos, the *xirp2a* labeling showed that the boundaries were shortened in the dorso-ventral axis, as shown in Figure 11D, while some embryos displayed *xirp2a* labeling that was discontinuous dorso-ventrally, suggesting a failure to form distinct boundaries between somites (Figure 11C). Finally, *xirp2a* expression was faint or not detected in the tip of the tail, suggesting a failure to form boundaries between the developing somites at 24 hpf.

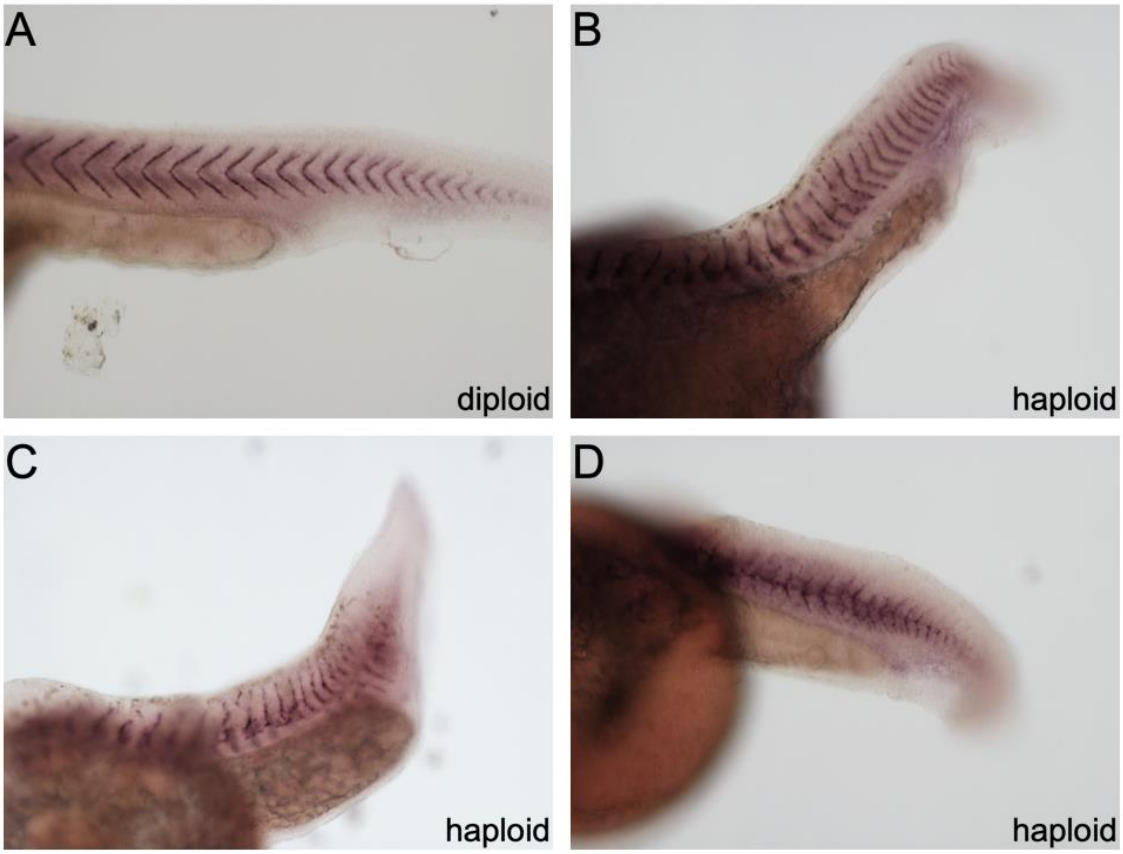

Figure 11. Defects in *xirp2a* expression in haploid embryos at 24 hpf. (A) Segment boundaries in a diploid embryo at 24 hpf. (B-D) Varying defects in segment boundaries of haploid embryos at 24 hpf. (n=12-17) All panels are at the same magnification.

Because the somitic boundaries showed development defects, somite development was further investigated by performing whole mount in situ hybridization using an antisense probe for the *myod1 (myogenic differentiation 1*) transcription factor. In control, diploid embryos, *myod1* was expressed in blocks that revealed the shape of the somites (Figure 12A). However, in haploid embryos, *myod1* expression was disrupted (Figure 12B, C). In the trunk, *myod1* expression was faint or undetected. Moderate staining was observed in the anterior tail adjacent to the yolk extension. By contrast, expression was strong in the posterior tail.

Here, distinct somites were not observed or were difficult to distinguish. This was consistent with the lack of *xirp2a* expression in this region.

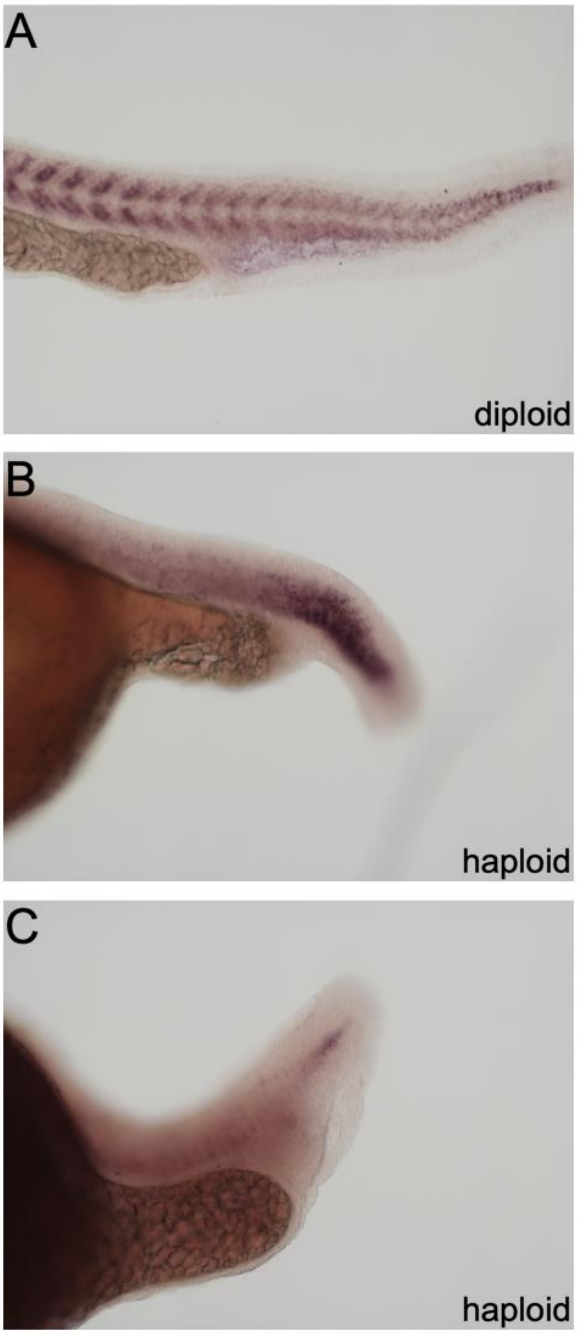

Figure 12. Defects in *myod1* expression in haploid embryos at 24 hpf. (A) Myogenic precursors in a diploid embryo. (B-C) Haploid embryos expressing disrupted *myod1* patterning. (n=17-20) All panels are at the same magnification.

Next, I asked whether these posterior defects would persist through later development or resolve. To address this, diploid and haploid embryos were grown to 32 hpf then fixed and processed for whole mount in situ hybridization. In diploid embryos, the chevron-shaped somitic boundaries were detected by labeling with *xirp2a*, but the labeling was more faint at 32 hpf than at 24 hpf (Figure 13A). This suggested that *xirp2a* gene expression was down-regulated by 32 hpf. In haploid embryos at 32 hpf, *xirp2a* expression was likewise faint and the boundary defects were consistent with those seen at 24 hpf (Figure 13B). Grossly, some embryos appeared to have longer tails than at 24 hpf, suggesting that there was significant posterior outgrowth. These tails showed lateral curvature, evidenced by an inability to achieve focus along the full length of the tail through the microscope. Because of this, images were taken at different z-positions to provide in-focus images of different regions of the tail. Panels B-B" show one specimen imaged at three focal planes to observe the extent of *xirp2a* expression along the tail, revealing that the boundary defects observed at 24 hpf persisted through 32 hpf. The developing somitic muscle could not be analyzed as labeling with *myod1* revealed no expression in diploid or haploid embryos at 32 hpf (Figure 13C-D).

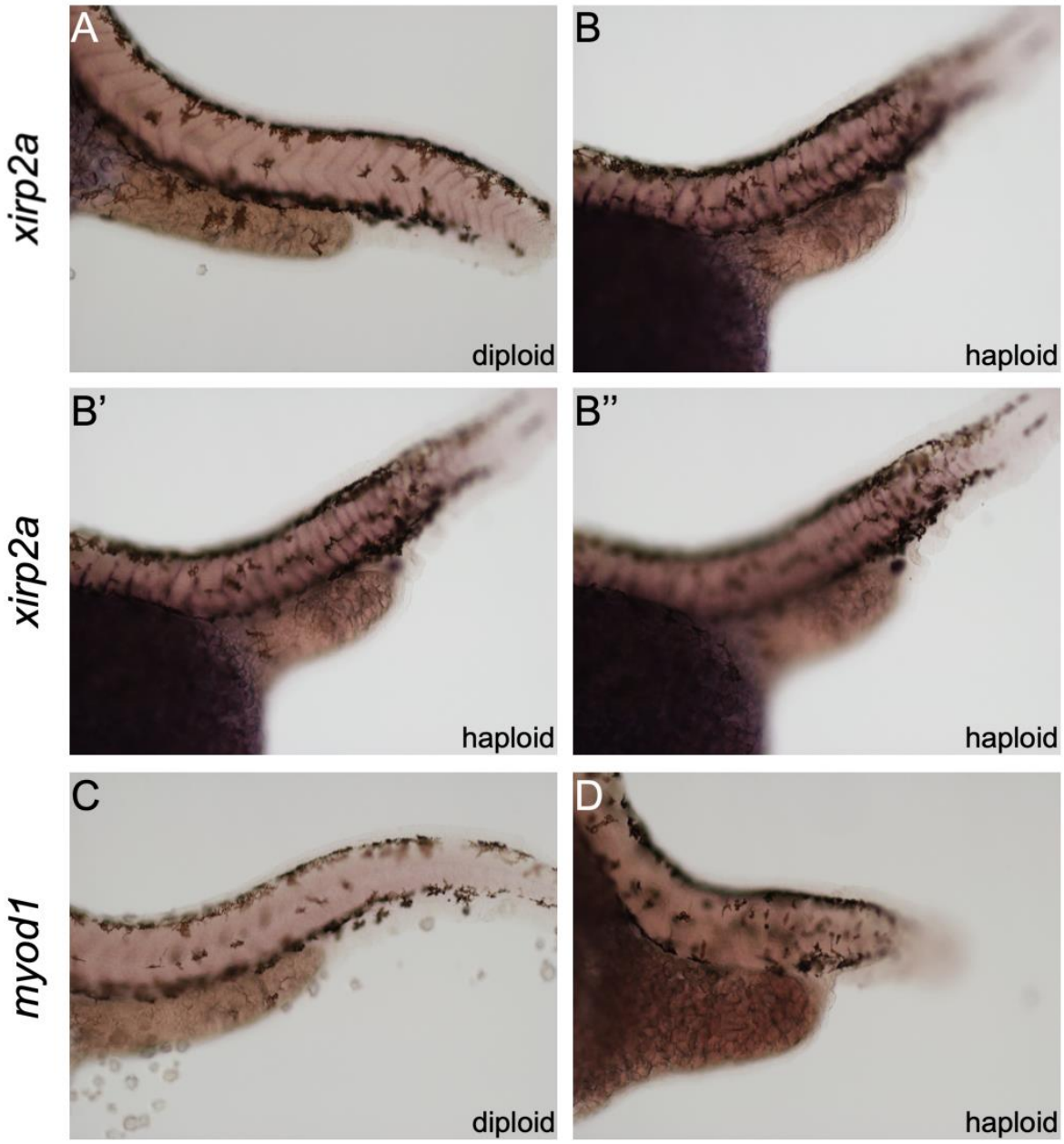

Figure 13. Gene expression at 32 hpf in diploid and haploid embryos. (A) Diploid embryo labeled with *xirp2a*. (B) Haploid embryo labeled with *xirp2a*. (B'-B'') The same specimen as (B) imaged at additional focal planes to observe the somitic mesoderm. Z-axis positions for B-B" are 1,880.19 µm, 1,860.56 µm, and 1,834.11 µm respectively. (C) Diploid embryo labeled with *myod1,* showing no expression. (D) Haploid embryo labeled with *myod1,* showing no expression. (n=20-25) All panels are at the same magnification.

Somite formation was investigated in tetraploid embryos. Again, whole mount in situ hybridization was performed using an antisense probe to detect *xirp2a* expression in the

somite boundaries. Given the range of morphological defects observed earlier (Figure 10), I predicted that there would be a range of defects in the formation of the somitic boundaries. Consistent with this, tetraploid embryos showed *xirp2a* staining with a range of patterns. Some embryos showed expression patterns that were not significantly different from that of control embryos (Figure 14A, B). However, embryos with gross morphology defects also exhibited apparent defects in their somitic boundaries. Commonly, the boundaries appeared more linear than chevron-shaped (Panels C, G). Some embryos showed boundaries that resembled the chevron pattern, but had shortened tails, as in Panels D and E. While the patterning appeared mostly normal for these embryos, it was evident that the somites were compressed compared to diploid embryos.

Another patterning irregularity in tetraploid embryos was asymmetry in gene expression of the posterior axis. For embryos that did not have much lateral curvature in the tail and were thus able to be laid evenly flat on a slide, it was possible to view the left and right sides of the tail by focusing up and down. This revealed asymmetrical *xirp2a* expression on the left versus right sides of the tail (Figure 14 panels F, F' and G, G'). In panel F, *xirp2a* showed distinct chevron-shaped expression on one side. However, imaging the other side of the tail revealed discontinuous *xirp2a* expression. Here, expression was punctate or absent in specific boundaries. Similarly, in panel G, while one side of the tail showed strong *xirp2a* expression with distinct somitic boundaries, the other side revealed disrupted expression along the dorso-ventral axis (panel G').

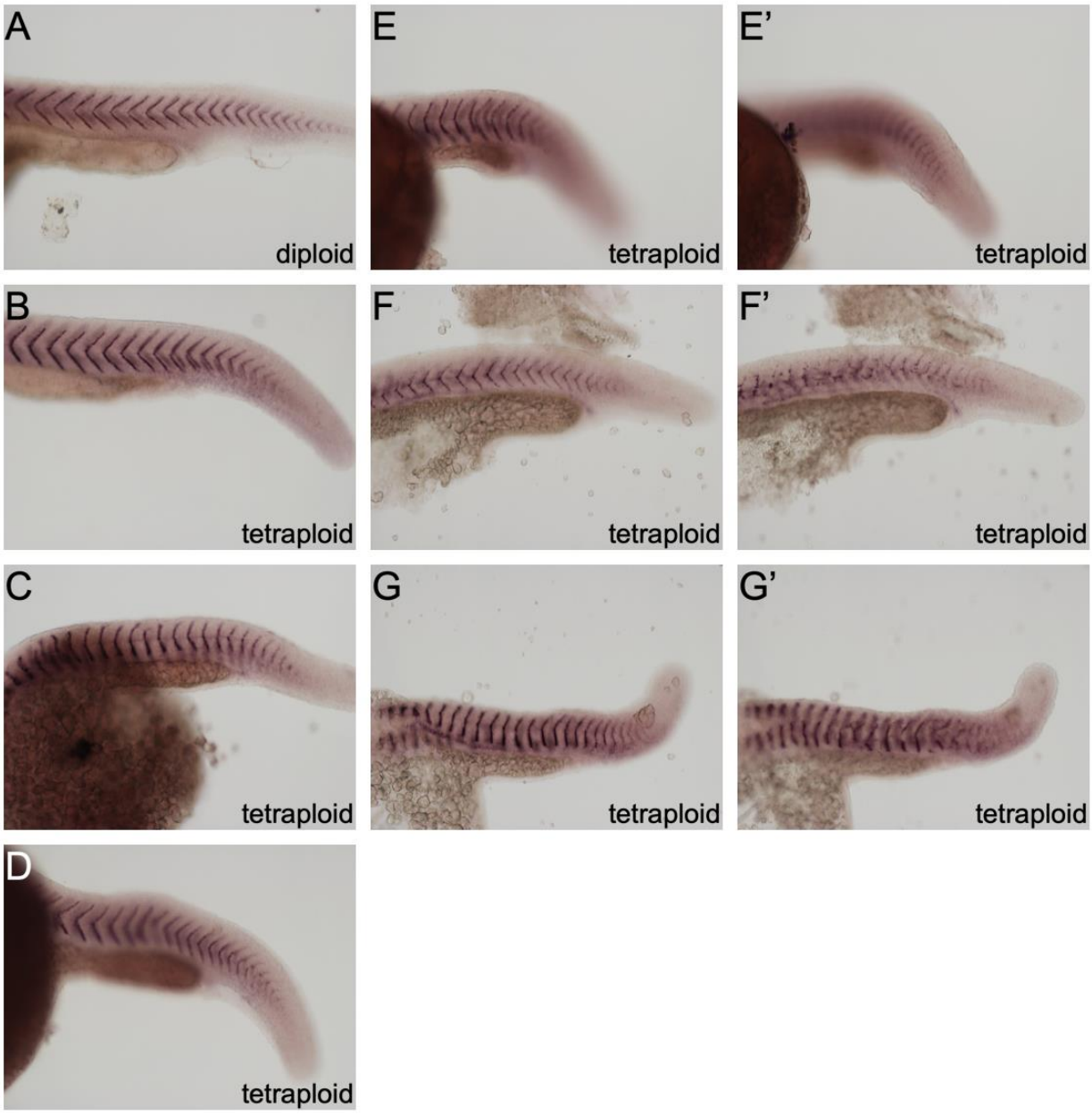

Figure 14. Somite boundary defects in tetraploid embryos at 24 hpf. (A) Gene expression pattern of *xirp2a* in a diploid embryo. This is the same image seen in Figure 10A. (B) A tetraploid embryo with chevron-shaped somitic boundaries, consistent with the diploid pattern. (C-G') Tetraploid embryos with shortened tails. (C) Tetraploid embryos with misshapen boundaries. (D) Tetraploid with a slight curve along the lateral axis and shortened somites. (E, E') Tetraploid embryo with shortened axis and curve along the tail. Z-axis position (E) 2,019.17 µm (E') 1,917.34 µm. (F-G') Tetraploid embryos with shortened tails and boundary asymmetry on left and right sides, with misshapen or missing boundaries. Z-axis position (F) 1,799.23 µm (F') 1,838.87 µm (G) 1,802.41 µm (G') 1,845.91 µm. (n=17-25) All panels are at the same magnification.

As with haploid embryos, tetraploids were hybridized with *myod1* to analyze the effects that changing ploidy had on the development of muscle precursors. Consistent with the range of expression patterns observed with *xirp2a* gene expression, there was a range in *myod1* expression patterns. Some tetraploid embryos showed *myod1* expression that was similar to that of diploid embryos (Figure 15A-C). In other tetraploid embryos, *myod1* expression was faint or absent in the trunk and anterior tail while showing intense expression at the tip of the tail (Figure 15D, E).

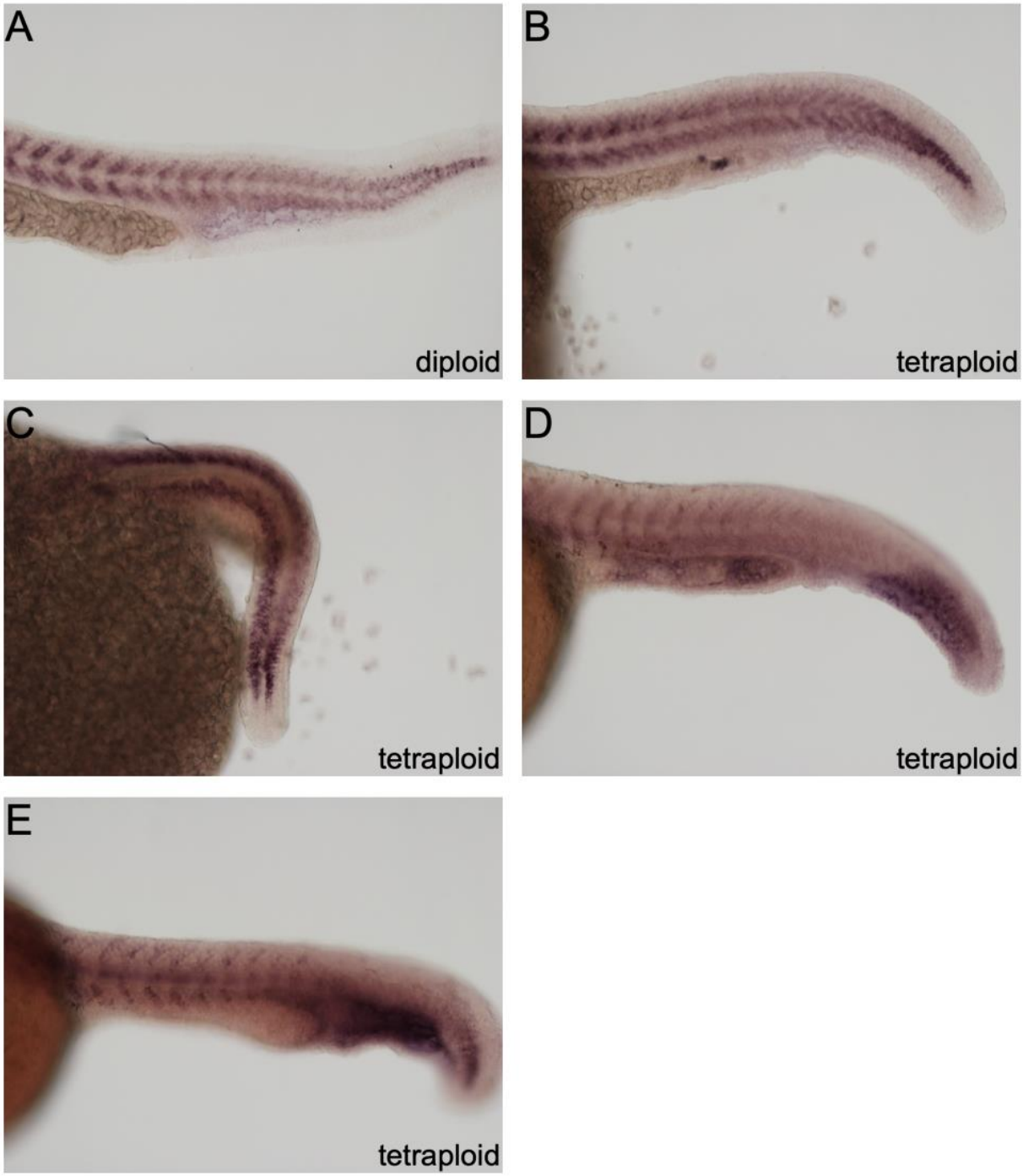

Figure 15. Defects in *myod1* expression in tetraploid embryos at 24 hpf. (A) *myod1* expression in a diploid embryo at 24 hpf. This is the same image seen in Figure 11A. (B) A tetraploid embryo with gene expression similar to the diploid embryo. (C-E) Tetraploid embryos expressed a variety of defects in *myod1* expression. (n=17-25) All panels are at the same magnification.

Tetraploid embryos were grown to 48 hpf and somitic gene expression was observed to determine whether the defects would persist. Embryos with severe gross defects did not have a high rate of survival past 24 hpf. Thus, the more moderately defective embryos survived to 48 hpf. In this subset, there was no expression of *xirp2a* at the somite boundaries, though segments were clearly defined and visible despite a lack of labeling (Figure 16A, B). The somite boundaries were similar to those seen in the tetraploid embryos with minimal defects at 24 hpf (Figure 14B). Additionally, *myod1* expression was not detected at 48 hpf for diploid or tetraploid embryos (Figure 16C, D).

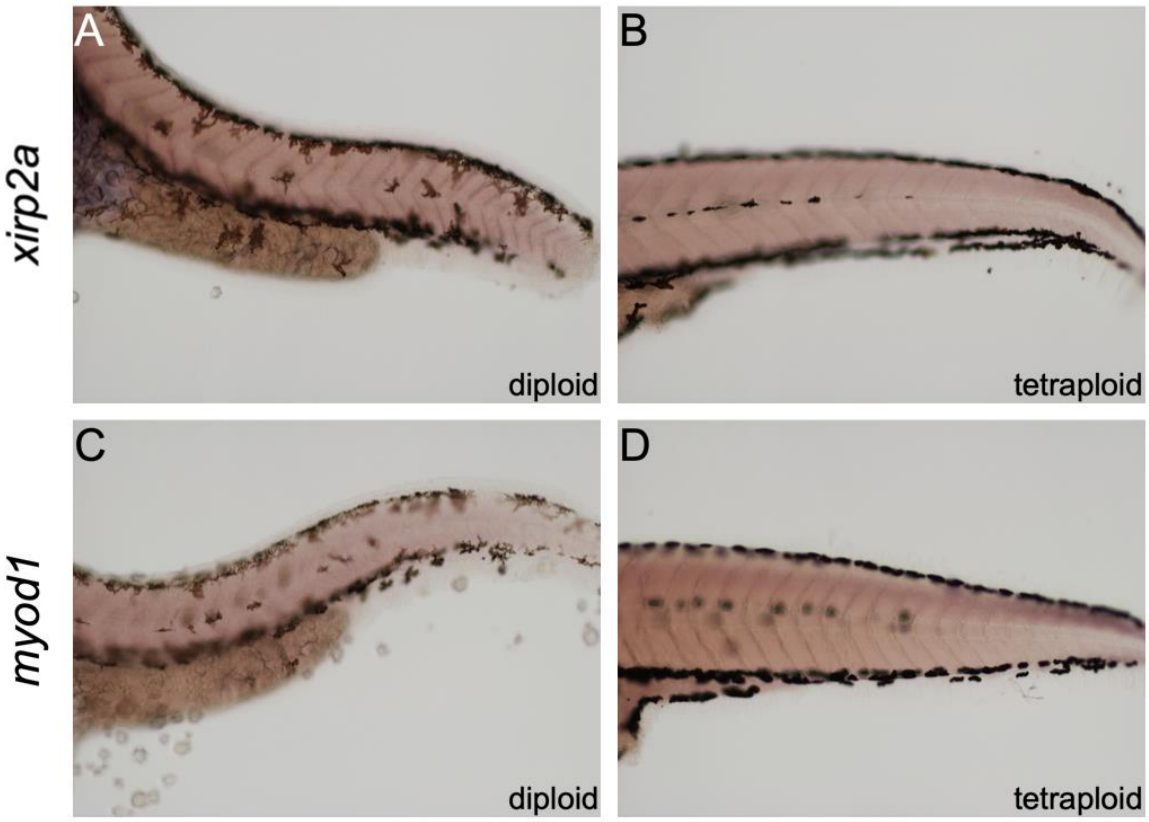

Figure 16. *xirp2a* and *myod1* expression in later stage embryos. (A and C) Diploid embryos at 32 hpf, same as those seen in Figure 12A and 12C (B and D) Tetraploid embryos at 48 hpf. (n=25-30) All panels are at the same magnification.

DISCUSSION

The focus of this study was to test the hypothesis that aneuploidy is associated with defects in posterior outgrowth and somite formation during embryonic development. Investigation began with the generation of aneuploid embryos and confirming that ploidy was altered as expected through karyotyping analysis. Observations of the gross morphologies of aneuploid embryos showed that altered ploidy resulted in embryos that had malformed posterior axes. Somite formation was analyzed through observations of gene expression. The results showed that somites in aneuploid embryos were defective in both their borders as well as in their tissue maturation. In all, this study showed that aneuploidy does cause defects in the posterior body of zebrafish embryos, both in their axis formation, as well as in the formation of somites.

Ploidy manipulation and karyotyping

Haploid embryos were generated through the manipulation of the sperm with UV irradiation prior to fertilization of the egg. UV irradiation crosslinks the DNA in the sperm, causing the sperm to be unable to contribute its genetic material. UV-treated sperm are able to trigger the fertilization response in the egg without the passage of genetic material to the egg, which will proceed into meiosis II and begin cell division. When used for fertilization, these irradiated sperm and untreated eggs created haploid embryos that only contained genetic material from the egg, as reported in previous studies (Westerfield, 2000; Kroeger et al., 2014).

During initial attempts of the UV-treatment, it was seen that diploid embryos were also present in the clutches of haploid embryos. This was confirmed through both

morphology and karyotyping. It was determined that when UV-treated sperm was returned to the initial tube, non-irradiated sperm must have been present. When the eggs are fertilized with that sample of sperm, then there are non-irradiated sperm present that fertilized eggs and generated diploid embryos. To address this, UV-treated sperm was held in a sterile centrifuge tube post-treatment, the fertilized embryos resulted in a 100% success rate generating haploid embryos. With a previously known and consistent appearance of haploid embryos at 24 hpf, the selection of these embryos required little guesswork when identifying haploid embryos. Further, these karyotyping results showed 25 chromosomes in the spreads from single cells. With a low chromosome count, there was little overlap between the chromosomes which allowed for easy counting and identification.

To investigate the effects of excess chromosomes, tetraploid embryos were generated. Tetraploid embryos, having double the DNA content of a wildtype diploid embryo, showed 100 chromosomes. Tetraploid embryos were produced through the heat shock of an early embryo. A heat shock during the later period of the first cell cycle (22-24 mpf) inhibits the duplication of the centrioles. By doing this, the second cell cycle division is disrupted, without the duplicated centrioles the cleavage furrow cannot form properly. Thus, heat shocks at 22 mpf resulted in the two blastomeres failing to divide during the second cell cycle, resulting in cells with double the amount of DNA content (Baars et al., 2016).

Due to the much higher chromosomal content in tetraploids, metaphase spreads that clearly resolved all 100 chromosomes were difficult to find due to the clumping and overlapping of chromosomes. Figure 7B and B', is a metaphase spread from a tetraploid embryo. Roughly 86 chromosomes were able to be individually counted. However, the clumping and overlapping in the chromosomes suggested more were present, confirming that

tetraploid embryos were created. Counting all 100 chromosomes was not possible when analyzing tetraploid metaphase spreads. Most samples from tetraploid embryos had chromosome counts well above 50, but due to the overlapping of chromosomes, there were no samples with all 100 chromosomes clearly resolved.

Additionally, confirmation of embryos that were appropriately stalled also made the isolation of tetraploid embryos difficult. Even if the embryos were heat shocked at the appropriate time, the studies outlining this method noted that not all embryos would be stalled as a result of the heat shock (Heier et al., 2015; Baars et al., 2016). Sorting through treated embryos for stalled embryos proved difficult for technical reasons including suboptimal lighting conditions with the available microscope combined with a large volume of embryos. To select embryos for karyotyping, 3-5 embryos were selected that reflected the extremes- those that appeared diploid, and those that were very deformed- while 8-10 embryos were selected randomly to limit the chance of bias. All these embryos were prepped for karyotyping and screened to confirm ploidy. Karyotyping ultimately confirmed the doubling of DNA content and the resulting morphological defects were consistent with the defects reported in the literature. (Menon et al., 2020; Heier et al., 2015). Thus, I conclude that tetraploid embryos were successfully generated using the heat shock method.

Gross morphology differences

After confirming that aneuploid embryos were successfully generated, the next step was to analyze posterior outgrowth and morphology at 24 hpf. Prim-5 denotes the wildtype developmental stage at 24 hpf. At this stage, the tail bud is small and surrounded by the tail fin primordium. During this period of development, the posterior axis is continually

straightening and begins a period of rapid lengthening that lasts until around 30-32 hpf (Kimmel et al., 1995). It is for these reasons that 24 hpf embryos were chosen for analysis of the posterior axis.

Diploid embryos at 24 hpf expressed straight anteroposterior axes with tails that extended well beyond the yolk sac extension. This is the control to which haploid and tetraploid embryos were compared. The gross morphology seen in haploid embryos reflected what was expected based on the literature. Haploid embryos have frequently been used for studies with homozygous recessive genes, so their morphology is well known (Westerfield, 2000; Kroeger et al., 2014). As seen in Figure 9B, haploid embryos had a severely shortened posterior body with tails that only extended slightly past the yolk sac extension. Many haploid embryos also showed a curvature of the posterior body and tail. These findings are consistent with previous reports (Streisinger et al., 1981; Kroeger et al., 2014).

While haploid embryos had a predictable and consistent set of morphological defects, tetraploids showed more variety in their gross morphologies. As referenced before, tetraploid embryos have been used to study the effects of cell size differences on development within a specific context. This all means that there is not a clear description of the deficiencies of tetraploid embryos in the literature. While the Menon et al., research article notes that tetraploids have "late developmental abnormalities" there are no specific descriptions. The figure provided to display these abnormalities shows variability in the malformed tetraploid embryos (Supplementary Fig. 3, Menon et al., 2020). Their primary focus was detailing the defects presented during gastrulation, and so little data focuses on the deficiencies seen later during development. What previous studies have noted was that tetraploid embryos had shortened body axes (Menon et al., 2020; Rodriguez, 2020). My results also showed this

shortened axis, as well as variability in the ways in which the bodies were shortened. While some tetraploid embryos appeared to be nearly normal morphologically, there were specimens with morphologies similar to what was seen in haploids with curved tails and shortened axes. Another common deviation from normal morphology was those embryos that appeared delayed by 2-4 hours such that, at 24 hpf, the embryos had developed to the 20 or 22 hpf stage, with no obvious morphological defects. Overall, despite the phenotypic variability, it was clear that the change in ploidy resulted in defects of the posterior body and its outgrowth.

Analysis of somite boundaries and gene expression in haploid embryos

A crucial element for proper body outgrowth is the development of somites. Previous studies have shown that when somite formation was disrupted, the posterior body also showed defects (Prajapati et al., 2020). To begin the investigation of somite development, *xirp2a* was utilized to visualize the somite boundaries. *Xirp2a* has shown to be useful when investigating the proper formation of somites. This marker indicates the myoseptum and thus marks the boundaries between somites (Thisse et al., 2004; Deniziak et al., 2007; Schröter et al., 2010). The diploid embryos at 24 hpf showed the clearly defined chevron pattern that can be expected from properly formed somites. However, in haploid embryos, instead of the chevron shape, the boundaries appeared to be more linear. Haploid embryos produced a segmented pattern but the somites themselves lacked proper shape. Measurements were not taken of individual somite lengths), but it is apparent that the haploid embryos have shorter somites compared to the diploid embryos. It should also be noted that the intensity of *xirp2a* expression was consistent with what was seen in the diploid embryo, having clear staining at

segment boundaries from the trunk of the embryo through to the tail. This suggests that somite boundaries were being formed in haploid embryos, but that the formation of somite shape, and therefore boundaries, was defective.

These results show that the general process of segmentation and the generation of somite boundaries was not disrupted, but defects in somite size and shape were apparent. The development of somites is highly dependent on the movement and interaction of cells within each somite and the cells at the borders. If these movements are disrupted, then it is reasonable to conclude that the formation of the segments would also be disrupted. When analyzing cell movement during gastrulation, Menon et al. (2020) found that haploid cells took significantly more tortuous paths during migration than diploid cells. The increase in tortuosity showed that haploid cells took more difficult paths, instead of following a more focused and linear migration path. Additionally, migrating haploid cells also expressed fewer membrane protrusions than diploid cells. These deficiencies are necessary to consider when analyzing the defects later seen in their development. Haploid cells cannot make the proper connections with one another and migrate to their positions effectively. This leads to the malformation that is seen in the somite shape in the haploid embryos. *Xirp2a* expression displays that the process of segmentation was accomplished in haploid embryos; however, the somites did not assume the proper chevron shape.

Somites are the precursors to several different tissue types, including skeletal muscle tissue. For analysis of somite maturation and the progression of tissue differentiation, *myod1,* was utilized (Weinberg et al., 1996; Zhang et al., 2018). In diploid embryos at 24 hpf, the striped gene expression pattern of *myod1* reflects the chevron shape of the somites, with lighter staining at the anterior of the trunk with slightly darker staining towards the tip of the

tail. When examining haploid embryos at 24 hpf, individual stripes of *myod1* expression were more difficult to identify. The staining was mostly absent in the trunk and staining in the tail was dark, but individual somites were not clearly demarcated.

As previously discussed, haploid cells have difficulty migrating properly. If cells cannot align along the axis properly, it is possible that cells are not receiving the proper positional cues that help guide differentiation. This could explain the absence of *myod1* staining in the trunk of the haploid embryos. The deficiencies in *myod1* staining somewhat mirror the *xirp2a* staining seen in haploid embryos. Towards the tip of the tail, the segment boundaries were very close together and less distinguishable. The lack of distinction between segments at the tail would explain the difficulty in identifying segments in the *myod1* staining. Further, the lack of staining in the trunk of haploid embryos is also of interest. At 24hpf, *myod1* staining is known to be significantly decreased in the trunk of the embryo, while staining remains darker towards the tail (Weinberg et al., 1996). Given that there is no obvious staining in the trunk of haploids, we can either conclude that trunk somites may experience an early down-regulation of gene expression or are failing to express the necessary genes for proper somite maturation. Either of these would contribute to the malformed somites seen in haploid embryos. Additionally, if the somites are failing to develop mature muscle tissue, this would also contribute to abnormal somite shape. In their work on muscle fibers and segment boundaries, Henry et al., found that as muscle fiber elongation is limited by somite boundaries (2005). With boundaries that are very close to one another as was seen with the *xirp2a* staining, this would explain the disorganized expression of *myod1* in the haploid embryos.

Analysis of somite boundaries and gene expression in tetraploid embryos

Just as was done with haploid embryos, I first looked at the segmentation pattern of tetraploid embryos using *xirp2a.* When examining the gross morphology of tetraploid embryos, it was noted that there was variability in the degrees of malformation in the posterior body. Some embryos appeared normal, with morphologies similar to diploid embryos, and others varied in abnormalities, some so severe that they somewhat resembled haploid morphologies. The variability that was seen in the morphology of tetraploid embryos was also seen in their somitic boundaries. There were embryos with boundaries that resembled the chevron shape seen in diploid embryos, while others had more linear boundaries. There was also variability in the symmetry of somite boundaries along the axes of some tetraploids. Some embryos showed boundaries that were more clearly defined on one lateral side of the tail than their counterparts on the other side of the axis. There were also embryos that displayed patchy patterning all along the axis from trunk to tail. These boundaries had breaks and irregular shaping in the boundaries. Though there were clear abnormalities, the intensity of the staining was consistent with that seen in diploid and haploid embryos. This reveals that segmentation was accomplished (with the exception of the subset of embryos that had patchy staining), but that the formation of the segments was disrupted in some way.

If proper cell migration and interactions are necessary for the creation of symmetry along the posterior axis, then the poor ability of tetraploid cells to migrate properly could explain why the asymmetry is seen at 24 hpf when looking at *xirp2a*. The tension and resistance mechanism proposed by Rost et al. (2014), suggests that the formation and control of the chevron shape in somites are based on cell rearrangements within the segments and

interactions with the segment boundaries. If proper maintenance of these cannot be held, the formation of the chevron shape will not take place, which is seen in many of the tetraploid embryos.

Tetraploid embryos also showed variability in *myod1* expression. However, in comparison to the haploid embryos, tetraploid embryo expression of *myod1* was more similar to the expression seen in the diploid embryos. They were more similar in that there is expression of *myod1* in the trunk of the embryos, with increasing intensity towards the tip of the tail. The major deviation from diploid expression was the irregular shape of the staining. In diploid embryos, the staining clearly resembled the chevron shape of the developing somites. In tetraploid embryos, segments were easily identified, but the shape of the segments was off. Some appeared like faint versions of the staining seen in diploids, but with much darker staining at the tip of the tail that lacked the definition of segments.

Unlike haploid embryos, tetraploid embryos were shown to have a clearer expression of *myod1* considering that there was clear staining in the trunk and the familiar intensity at the tip of the tail. Many tetraploid embryos had a longer posterior axis than haploid embryos. When considering that positional identity is better laid out when the axis is closer to proper proportion, this could explain the more efficient *myod1* staining seen in the tetraploid embryos. The abnormalities in the formation of the somites mirror the defects seen in the boundaries of the tetraploid embryos. As was discussed with the haploid embryos, if cells cannot properly migrate through the embryo, this will result in defects in the growing posterior axis. Additionally, given that developing muscle fibers are limited by the somite boundaries, the abnormal *myod1* expression is limited by the abnormal boundaries seen in the

tetraploid embryos. All this supports the hypothesis that posterior patterning is disrupted by aneuploidy.

Analysis of later-stage embryos

Further investigation of aneuploidy effects on posterior development was made through the analysis of later-stage embryos at 32 and 48 hpf. A look at gross morphology showed that the haploid and tetraploid embryos did not have additional gross defects. Analysis of gene expression at these later time points provided less information other than a down-regulation in expression from the 24 hpf time point in both diploid and aneuploid embryos. All embryos processed through *in situ* hybridization were developed in the NBT/BCIP for the same amount of time, regardless of stage. Strong staining was observed in all ploidies at the 24 hpf stage. Because there is no evident staining in the later-stage embryos after the same incubation period, it is clear that expression of both *xirp2a* and *myod1* were downregulated since 24 hpf. Research shows that at these later time points in wildtype diploid embryos, both genes are still being expressed in wildtype embryos (Weinberg et al., 1996; Lin et al., 2006; Deniziak et al., 2007; Schröter and Oates, 2010). In order to visualize if gene expression is aberrant in aneuploid embryos at the later age point, it would be necessary to allow the embryos to incubate in the NBT/BCIP until staining was visualized. Despite the lack of information from the gene expression analyses, it was clear that the embryos with manipulated ploidies expressed deformities in their morphologies.

Conclusions

Previous studies confirmed that altering ploidy results in a gross change in cell size (Menon et al., 2020; Rodriguez, 2020). Analyses from this study showed that the posterior formation of embryos was disrupted as a result of aneuploidy. The defects seen in aneuploid embryos were further revealed in gene expression analysis, which showed that somite formation was perturbed. Many recent studies have shifted focus to the influence of mechanics on posterior development. Many of these have investigated the negative effects that occur when cells cannot migrate properly or when tension or interactions between cells/tissues are disrupted. As a gross change in cell size is a characteristic of cells with altered ploidy, this suggests that cell size defects contribute to the malformations of the posterior body that are seen in aneuploid embryos. If cells are not properly positioned within the presomitic mesoderm, this could explain the defects that are seen in the development of the posterior axis. Further, if cells cannot maintain the proper forces of tension and resistance, this can lead to deformed somites and asymmetry along the axis. All of this supports the finding that the defects seen in the posterior body and in somite formation were the result of aneuploidy.

Future directions

To better understand the degree to which aneuploidy has disrupted somite formation, it would be useful to determine the somite length for each in the aneuploid embryos. Somite length is mentioned in the literature but is primarily focused on studies examining the period of somite formation and external influences such as temperature (Schröter et al., 2008). While it is clear that somite length is shortened in haploids and some tetraploids, having

precise measurements may allow insight into the extent of aneuploidy's change in somite development. Along with somite length, somite count is also of interest. It has previously been noted that haploid zebrafish embryos have the same number of somites as diploid embryos, but there is presently not any data that confirms the somite count for tetraploid embryos (Walker, 1999). It would be important to note if there are differences in somite number in tetraploids, as that could guide us in determining when some of the defects begin, as somite formation is pre-patterned in the PSM. This could provide clarity as to if the abnormalities in tetraploids are more dependent on gene expression disruption or mechanical issues as posited in this study. Even delays in the period of the segmentation clock due to inefficient cell movements could result in abnormal somite length and number (Shröter and Oates, 2010).

Additionally, to better analyze the deficiencies in tetraploids, it would be necessary to develop a more careful and controlled sorting method of tetraploid embryos, to ensure that the embryos being observed are actually of that ploidy. With poor lighting and too many embryos to sort through at once, it was difficult to be certain that sorting was accomplished properly. Karyotyping showed that some embryos that were sorted into the “stalled” category were actually diploid embryos. More efficient sorting will provide more confidence in any findings regarding tetraploid embryos.

To determine if aneuploidy is affecting the differentiation of the somites, quantitative PCR could be performed using common somite markers to determine if their respective levels are being disrupted. Examples of these markers could include *fgf8*, *smyhc*, *pcdh8*, and *tbx6*. This could assist in determining what factors of aneuploidy are having a more direct impact on posterior formation: the altered chromosome number or altered cell size.

Investigating the extracellular matrix could also reveal what deficiencies in cell-matrix connections between somites could be affected due to the change in ploidy. Gene expression analysis or immunohistochemistry with antibodies for proteins of interest, such as fibronectin or laminin, could offer insight into aneuploid cells' ability to create somite boundaries. These could lend to the argument that surface tension and the resistance created amongst cells in a tissue are no longer being supported, leading to malformations in the posterior body.

Menon et al. determined that altered cell size resulted in defects in cell migration during gastrulation (2020). To investigate the influence of cell migration during the somitogenesis period, a time-lapse of cell migration in the PSM could be performed. This would provide insight as to whether or not the defects in cell migration are persistent through development.

REFERENCES

Asana Marican, H. T., Sun, L. W. H. and Shen, H. (2021). A simple method to establish metaphase chromosomes from individual zebrafish embryos. *Zebrafish* 18, 338–341.

Baars, D. L., Takle, K. A., Heier, J. and Pelegri, F. (2016). Ploidy manipulation of zebrafish embryos with heat shock 2 treatment. *J Vis Exp*. 118, e54492.

Bhavna, R. (2020). Segmentation clock dynamics is strongly synchronized in the forming somite. *Dev Biol* 460, 55–69.

Cooke, J. and Zeeman, E. C. (1976). A clock and wavefront model for control of the number of repeated structures during animal morphogenesis. *J Theor Biol* 58, 455–476.

Deniziak, M., Thisse, C., Rederstorff, M., Hindelang, C., Thisse, B. and Lescure, A. (2007). Loss of selenoprotein N function causes disruption of muscle architecture in the zebrafish embryo. *Exp Cell Res* 313, 156–167.

Dubrulle, J. and Pourquié, O. (2004). Coupling segmentation to axis formation. *Development* 131, 5783–5793.

Heier, J., Takle, K. A., Hasley, A. O. and Pelegri, F. (2015). Ploidy manipulation and induction of alternate cleavage patterns through inhibition of centrosome duplication in the early zebrafish embryo. *Dev Dyn* 244, 1300–1312.

Henry, C. A., McNulty, I. M., Durst, W. A., Munchel, S. E. and Amacher, S. L. (2005). Interactions between muscle fibers and segment boundaries in zebrafish. *Dev Biol* 287, 346–360.

Holley, S. A. (2007). The genetics and embryology of zebrafish metamerism. *Dev Dyn* 236, 1422–1449.

Kimelman, D. (2016). Tales of tails (and trunks): Forming the posterior body in vertebrate embryos. *Curr Top Dev Biol* 116, 517–536.

Kimmel, C. B., Ballard, W. W., Kimmel, S. R., Ullmann, B. and Schilling, T. F. (1995). Stages of embryonic development of the zebrafish. *Dev Dyn* 203, 253–310.

Kroeger, P. T., Poureetezadi, S. J., McKee, R., Jou, J., Miceli, R. and Wingert, R. A. (2014). Production of haploid zebrafish embryos by in vitro fertilization. *J Vis Exp* 89, e51708.

Lin, C.-Y., Yung, R.-F., Lee, H.-C., Chen, W.-T., Chen, Y.-H. and Tsai, H.-J. (2006). Myogenic regulatory factors Myf5 and Myod function distinctly during craniofacial myogenesis of zebrafish. *Dev Biol* 299, 594–608.

McLaren, S. B. P. and Steventon, B. J. (2021). Anterior expansion and posterior addition to the notochord mechanically coordinate zebrafish embryo axis elongation. *Development* 148, dev199459.

Menon, T., Borbora, A. S., Kumar, R. and Nair, S. (2020). Dynamic optima in cell sizes during early development enable normal gastrulation in zebrafish embryos. *Dev Biol* 468, 26–40.

Naganathan, S. R. and Oates, A. C. (2020). Patterning and mechanics of somite boundaries in zebrafish embryos. *Semin Cell Dev Biol* 107, 170–178.

Naganathan, S. R., Popović, M. and Oates, A. C. (2022). Left–right symmetry of zebrafish embryos requires somite surface tension. *Nature* 605, 516–521.

Oates, A. C., Morelli, L. G. and Ares, S. (2012). Patterning embryos with oscillations: structure, function and dynamics of the vertebrate segmentation clock. *Development* 139, 625–639.

Prajapati, R. S., Mitter, R., Vezzaro, A. and Ish-Horowicz, D. (2020). Greb1 is required for axial elongation and segmentation in vertebrate embryos. *Biol Open* 9, bio047290.

Rodriguez, E. J. (2020). Manipulating chromosomal content in zebrafish embryos and determining the effects on differentiation of neuromesodermal progenitor cells. *MS Thesis*, Appalachian State University, Boone, NC.

Rost, F., Eugster, C., Schröter, C., Oates, A. C. and Brusch, L. (2014). Chevron formation of the zebrafish muscle segments. *J Exp Biol* 217, 3870–3882.

Sawada, A., Fritz, A., Jiang, Y.-J., Yamamoto, A., Yamasu, K., Kuroiwa, A., Saga, Y. and Takeda, H. (2000). Zebrafish Mesp family genes, mesp-a and mesp-b are segmentally expressed in the presomitic mesoderm, and Mesp-b confers the anterior identity to the developing somites. *Development* 127, 1691–1702.

Schröter, C. and Oates, A. C. (2010). Segment number and axial identity in a segmentation clock period mutant. *Curr Biol* 20, 1254–1258.

Schröter, C., Herrgen, L., Cardona, A., Brouhard, G. J., Feldman, B. and Oates, A. C. (2008). Dynamics of zebrafish somitogenesis. *Dev Dyn* 237, 545–553.

Stickney, H. L., Barresi, M. J. and Devoto, S. H. (2000). Somite development in zebrafish. *Dev Dyn* 219, 287–303.

Streisinger, G., Walker, C., Dower, N., Knauber, D. and Singer, F. (1981). Production of clones of homozygous diploid zebra fish (Brachydanio rerio). *Nature* 291, 293–296.

Thisse, B., Heyer, V., Lux, A., Alunni, V., Degrave, A., Seiliez, I., Kirchner, J., Parkhill, J.-P. and Thisse, C. (2004). Spatial and temporal expression of the zebrafish genome by large-scale in situ hybridization screening. In *Methods Cell Biol* 77, 505–519.

Uriu, K., Liao, B.-K., Oates, A. C. and Morelli, L. G. (2021). From local resynchronization to global pattern recovery in the zebrafish segmentation clock. *Elife* 10, e61358.

van de Pol, I. L. E., Hermaniuk, A. and Verberk, W. C. E. P. (2021). Interacting effects of cell size and temperature on gene expression, growth, development and swimming performance in larval zebrafish. *Front Physiol* 12, e738804.

Walker, C. (1999). Haploid screens and gamma-ray mutagenesis. *Methods Cell Biol* 60, 43–70.

Weinberg, E. S., Allende, M. L., Kelly, C. S., Abdelhamid, A., Murakami, T., Andermann, P., Doerre, O. G., Grunwald, D. J. and Riggleman, B. (1996). Developmental regulation of zebrafish MyoD in wild-type, no tail and spadetail embryos. *Development* 122, 271–280.

Westerfield, M. (2000). *The Zebrafish Book. A Guide For The Laboratory Use Of Zebrafish (Danio rerio)*. 4th ed., Univ. of Oregon Press, Eugene.

Wolpert, L., Jessel, T., Peter, L., Meyerowitz, E., Robertson, E. and Smith, J. (2007). *Principles of Development*. Third. Oxford University Press.

Yabe, T. and Takada, S. (2016). Molecular mechanism for cyclic generation of somites: Lessons from mice and zebrafish. *Dev Growth Differ* 58, 31–42.

Zhang, L., Yang, Y., Li, B., Scott, I. C. and Lou, X. (2018). The DEAD box RNA helicase Ddx39ab is essential for myocyte and lens development in zebrafish. *Development* dev.161018.

Vita

Abigail Shaw Hockett was born in Greensboro, North Carolina to David and Kim Hockett. She graduated from Jay M. Robinson high school in 2015. She began her studies at Furman University in the fall of 2015. There she graduated with a B.A. in Religious Studies, while also fulfilling the pre-medicine track. Post-graduation, she spent 8 months living in San Pedro Sula, Honduras where she worked with a non-profit assisting with children's homes. On her return in 2020, Abigail began her studies for a Master of Science degree with a concentration in Cell and Molecular biology where she is scheduled to graduate in May 2023.